minerals

MDPI

Article

Characteristics of Fluid Inclusions and Hydrocarbon Accumulation Stages of Carbonate Rock Reservoir: A Case Study from the Majiagou Formation Ordovician, Central and Eastern Ordos Basin

Yanzhao Liu [1], Zhanli Ren [1,2,*], Kai Qi [1], Xinyun Yan [3], Beile Xiong [4], Jian Liu [1], Junfeng Ren [5], Guangyuan Xing [1], Mingxing Jia [1], Juwen Yao [1] and Hongwei Tian [1]

[1] Department of Geology, Northwest University, Xi'an 710069, China; 202221638@stumail.nwu.edu.cn (Y.L.); qikai0913@163.com (K.Q.); liujian@stumail.nwu.edu.cn (J.L.); 202310408@stumail.nwu.edu.cn (G.X.); 202233549@stumail.nwu.edu.cn (M.J.); yaojuwen@outlook.com (J.Y.); tianhongwei1023@icloud.com (H.T.)
[2] Xi'an Key Laboratory of Multiple Energy Resources Exploration and Development, Xi'an 710069, China
[3] Research Institute of Exploration and Development, PetroChina Yumen Oilfield Company, Jiuquan 735000, China; ymyanxy@petrochina.com.cn
[4] Yumen Oilfield Branch Huanqing Oil Production Plant, Qingyang 745700, China; ymxbl@petrochina.com.cn
[5] Research Institute of Exploration and Development, PetroChina Changqing Oil Field Company, Xi'an 710018, China; rjf_cq@petrochina.com.cn
* Correspondence: renzhanl@nwu.edu.cn

Abstract: The Ordovician carbonate formations in the Ordos Basin provide a crucial stratigraphic unit for prospective oil and gas exploration. Significant progress has been made in the exploration of natural gas within the Ordovician subsalt formations. Nonetheless, understanding its accumulating properties requires additional investigation. Clarifying the formation periods of the carbonate rock reservoirs in the Majiagou Formation of the basin can furnish a theoretical foundation for advanced exploration of carbonate rock oil and gas. This study uses fluid inclusion petrography, laser Raman spectroscopy, and microscopic temperature measurement methods, along with information about the basin's history of burial and thermal evolution, to look at the oil and gas charging periods of Majiagou Formation reservoir in the central-eastern basin. The results show that there are two stages of hydrocarbon inclusions. The first stage has blue fluorescence and temperature peaks between 85 and 95 °C in the central basin and between 105 and 115 °C in the eastern basin. For the second stage, no fluorescence can be observed. Meanwhile, the temperature peaks are between 175 and 185 °C in the central basin, and between 165 and 175 °C in the eastern basin. In the central part of the basin, oil charging began in the Late Triassic (231–203 Ma) and reached the gas generation stage in the Late Early Cretaceous (121–112 Ma), peaking in natural gas charging. In contrast, the reservoirs in the eastern part of the basin experienced a primary oil charging stage in the Early Jurassic (196–164 Ma) and entered the gas generation stage in the Late Early Cretaceous (110–101 Ma). The hydrocarbon charging process in the study area is mainly controlled by the thermal evolution history of the basin. The study determines that the central basin enters the threshold of hydrocarbon generation earlier than the eastern basin, leading to earlier oil and gas charging.

Keywords: hydrocarbon accumulation stages; thermal evolution history; deep to ultra-deep; Majiagou Formation; Ordovician; Ordos Basin

check for updates

Academic Editor: Jan Golonka

Received: 13 December 2024
Revised: 26 January 2025
Accepted: 27 January 2025
Published: 30 January 2025

Citation: Liu, Y.; Ren, Z.; Qi, K.; Yan, X.; Xiong, B.; Liu, J.; Ren, J.; Xing, G.; Jia, M.; Yao, J.; et al. Characteristics of Fluid Inclusions and Hydrocarbon Accumulation Stages of Carbonate Rock Reservoir: A Case Study from the Majiagou Formation Ordovician, Central and Eastern Ordos Basin. *Minerals* **2025**, *15*, 139. https://doi.org/10.3390/min15020139

Copyright: © 2025 by the authors. Licensee MDPI, Basel, Switzerland. This article is an open access article distributed under the terms and conditions of the Creative Commons Attribution (CC BY) license (https://creativecommons.org/licenses/by/4.0/).

1. Introduction

Despite the current relatively low exploration level of deep oil and gas in China, the deep-to-ultra-deep carbonate formations, which are a new frontier for oil and gas exploration, hold substantial exploration potential. Through continuous exploration efforts, China has made remarkable progress in the domain of deep and ultra-deep oil and gas exploration [1].

The deep-to-ultra-deep carbonate formations are a new field of oil and gas exploration. The current exploration level of deep oil and gas in China is rather low; however, the potential for exploration is substantial. With continuous advancements in exploration efforts, China has achieved significant progress in the field of deep and ultra-deep oil and gas exploration [1]. Ordos Basin, located in central and western China, is one of the large craton basins in East Asia. Several gas fields such as Sulige, Jingbian, and Daniudi are developed in the basin, and natural gas comes from gas-producing strata widely developed in the region. The deep–ultra-deep carbonate strata are the main target horizon for natural gas exploration in Ordos Basin [2,3], the identification of substantial industrial gas flow in Ordovician Majiagou Member 4 (Ma 4) of Well MT1 in the eastern basin has marked a significant advancement in pre-salt natural gas exploration. In recent years, 108 exploration wells have penetrated the Ordovician Majiagou Formation, including seven gas-producing wells and 47 gas-bearing wells, which indicates that the carbonate exploration potential of this group is tremendous [4,5].

The Ordovician Majiagou Formation in the central and eastern part of Ordos Basin has undergone multiple stages of tectonic movement, during which the late transformation deformation is strong. There are significant differences in reservoir formation characteristics in different regions, so it is difficult to explore oil and gas. Therefore, it is necessary to restore its oil–gas accumulation history. The study of the hydrocarbon charging stages is essential for understanding the history of hydrocarbon accumulation and for defining its characteristics. The process of oil and gas charging is affected by tectonic movements, formation pressure, and temperature change, and is closely related to tectonic evolution. The determination of oil and gas charging time is helpful to reveal the time series of hydrocarbon accumulation, and it can also help to predict the phase state and distribution law of oil and gas in different charging stages. However, the Lower Paleozoic strata in the central and eastern parts of the basin have seen several episodes of tectonic deformation, and the environment for oil and gas accumulation is complex, resulting in certain differences in accumulation characteristics across different regions. The study of the hydrocarbon charging stages is essential for understanding the history of hydrocarbon accumulation and is crucial for defining the characteristics of hydrocarbon accumulation. Previous studies mainly focused on the characteristics of source rocks [2,6], sedimentary evolution [7,8], natural gas origin [4,5,9], and tectonic evolution [10,11] but were relatively weak in hydrocarbon accumulation and reservoir forming rule. The homogenization temperature of oil and gas inclusion can represent the formation temperature in the process of oil and gas charging, and its peak temperature can also reflect the peak oil and gas entering the reservoir. The pressure and composition of fluid inclusions can also reflect the reservoir environment. This information can determine when oil and gas entered the reservoir, so fluid inclusions are widely used in the study of oil and gas accumulation history [12]. Prior researchers employed techniques such as inclusion temperature measurement, thermal evolution history reconstruction, and hydrocarbon production history simulation to investigate the hydrocarbon accumulation stages of carbonate reservoirs in the Majiagou Formation of the basin. The primary perspectives are as follows: (1) The development of Ordovician reservoirs in the basin occurred in three stages: Jurassic, Early Cretaceous, and Late Cretaceous. The Jurassic period was the primary stage of reservoir development,

while the gas reservoir originated from oil cracking during the Cretaceous period [13]. (2) The hydrocarbon charging process of Majiagou reservoirs in the central region can be divided into two distinct periods: the liquid hydrocarbon charging stages prior to the Early Cretaceous and the gaseous hydrocarbon charging stages commencing from the Early Cretaceous [14,15]. (3) The natural gas charging process of Majiagou Formation has three separate stages. The initial stage transpired in the Late Triassic, the subsequent stage spanned from the Middle Jurassic to Early Cretaceous, and the final stage took place at the conclusion of the Early Cretaceous [16]. (4) Natural gas charging in the central basin occurs in at least two episodes, corresponding to the end of the Late Triassic and late Early Cretaceous periods, respectively [17]. The accumulation time of Majiagou Formation marine reservoir remains contentious, hindering deep carbonate gas development in the basin. Consequently, it is imperative to conduct additional research on the hydrocarbon accumulation period of Majiagou Formation reservoir in the central and eastern regions of basin.

The study of Majiagou Formation reservoir, specifically the SC1 and MT1 Wells in the central and eastern regions of this basin, employs petrographic observation, fluid inclusion composition analysis, homogenization temperature measurement, and basin thermal history simulation. Based on previous research, the aim was to investigate the oil–gas accumulation periods within these reservoirs and analyze the differences in these periods across these regions. The research results help clarify the reservoir accumulation characteristics of Majiagou Formation, providing a certain reference value for oil and gas exploration in the Early Paleozoic of the study area and its adjacent regions.

2. Geological Setting

The Ordos Basin is located in the western part of the North China Plate, is the second largest petroleum-bearing sedimentary basin in China (Figure 1a) [18]. The basin covers an area of about 2500 km^2, and the total thickness of the sediment is about 4000–6000 m [6]. The basin is delineated by the Yinshan orogenic belt to the north, the Qinling orogenic belt to the south, the Helan Shan-Liupanshui tectonic belt to the west, and the Luliang tectonic belt to the east.

The Ordos Basin is divided into six tectonic units, namely Western Thrust Zone, Tianhuan Depression, Central Paleouplift, Yishan Slope, Jinshaan Tectonic Zone, Yimeng Uplift, and Weibei Uplift. The basin exhibits tectonic characteristics such as activity in the periphery, relative stability within the basin, uplift in the north and south, and thrusting in the eastern and western directions, and regional distribution is characterized by high in the east and low in the west (Figure 1c) [6,10,11].

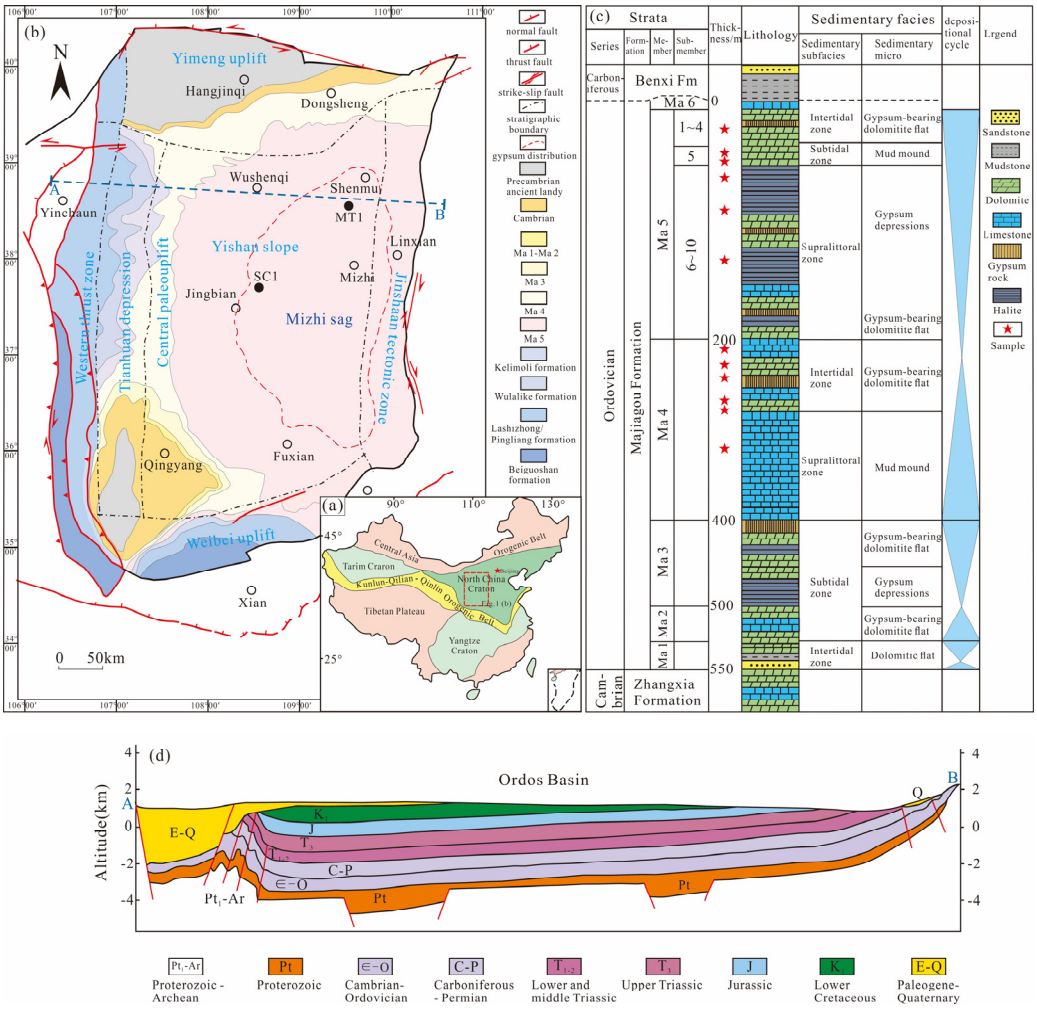

Figure 1. Geological map of Ordos Basin: (**a**) China's onshore plate tectonic map (modified from Liu et al., 2024 [19]); (**b**) geological map of the Pre-Cambrian–Ordovician system of Ordos Basin (modified from He et al., 2022 [4]); (**c**) stratigraphic column of Majiagou Formation (modified from Liu et al., 2024 [7]); (**d**) east–west trending simplified geological profile of the Ordos Basin (modified from Peng et al., 2023 [20]).

The basement of Ordos Basin is composed of Archean and paleoproterozoic metamorphic rocks, and the basin has undergone four major tectonic stages since the Mesoproterozoic: (1) The Ordos Basin was in the stage of rift basin dominated by tensioning in the Mesoproterozoic; (2) basin margin rift and intracontinental depression in Late Proterozoic to Middle Ordovician; (3) the Middle Ordovician and Middle Triassic were cratonic basins with convergent margins; (4) the basin margin was uplifted and tilted to the west during the Late Triassic and Early Cretaceous; (5) during the Cenozoic period, strong faulting activity occurred around the basin, and the whole tectonic pattern of the basin was completely formed [21–23]. The Ordovician Majiagou Formation is predominantly located in the central and eastern region of the basin (Figure 1a); its sedimentary period was affected by tectonic uplift and subsidence, resulting in periodic fluctuations in water levels inside the central depression. This led to the rhythmic deposition of continental and marine carbonate rocks, as well as confined marine gypsum–salt formations. This stratum has an unconformity contact with the lower Cambrian and the overlying Carboniferous [8]. The Ordovician Majiagou Formation can be stratified into six lithologic segments, ranging from the Ma 1 at the base to the Ma 6 at the top, based on lithology and depositional cycles [24]. Throughout the transgression period, the central and eastern regions of the

basin predominantly accumulated open platform limestone and dolomite, deposited by the Ma 2, Ma 4, and Ma 6, respectively. During the regressive period, the basin was mainly composed of gypsum rock and dolomite of platform facies with limited evaporation, that is, Ma 1, Ma 2, and Ma 5. In the sedimentary phase of Ma 4, the basin exhibited three principal uplifts from the west to east: the Central Palaeouplift, the Wusenqi Palaeouplift, and the subsalt low uplift. Among these uplifts lay the Taolimiao sag and the Mizhi sag, illustrating a complex structural configuration of "three ridges and two depressions" [14,25]. During the Ordovician period, the alternating transgressions and regressions that the basin experienced led to the formation of interbedded carbonate rocks and mudstones rich in organic matter, giving rise to source rocks [3].

A petroleum system encompasses several hydrocarbon accumulation elements, namely source rocks, reservoirs, traps, seals, migration pathways, and caprocks [26]. The Ordovician petroleum system in the Ordos Basin mainly includes two types of hydrocarbon accumulation associations: "source-reservoir-in-one" and "source-above-reservoir". (1) The "source-reservoir-in-one" assemblage refers to the accumulation of natural gas generated from the Ordovician carbonate source rocks in the dolomites within the salt sag. The source rocks of this type of hydrocarbon accumulation combination are mainly gypsum-bearing carbonate rocks and argillaceous dolomites. The organic matter types are mainly marine sapropel and humus dominated by algae (Type I kerogen and Type II_1 kerogen), with a content of approximately 3.3 wt%, and the vitrinite reflectance is about 2%–3%. The widely developed dissolution pores, cavities, and micro-fractures within the strata serve as the reservoir and migration spaces for natural gas [3,9]. (2) The "source-above-reservoir" assemblage means that the natural gas generated from the Carboniferous–Permian coal-measure source rocks migrates laterally to the Ordovician reservoirs through the unconformity surface [27]. The natural gas in this type of hydrocarbon accumulation combination is mainly coalbed methane, and its potential source rocks are the Carboniferous–Permian coal-measure strata. The thickness of the coal seams ranges from 2 m to 20 m. The weathering crust overlying the strata serves as an excellent caprock for the natural gas reservoirs [28].

In Ordovician Majiagou Formation, the upper natural gas accumulation association of Ma 5_6 of Majiagou Formation is called the "upper salt" paleokarst weathering crust gas reservoir. This type of gas reservoir belongs to the "source-above-reservoir" accumulation assemblage. The lower part of the Ma 5_6 Member is called the "subsalt" natural gas accumulation assemblage, and this belongs to the "source-reservoir-in-one" type of natural gas reservoir. The primary gas-producing intervals of Majiagou Formation are Ma 4 and Ma 3. The gypsum rock layer developed in the Ma 5_6 Member is characterized by large thickness, wide distribution area, and strong sealing ability, and it is the regional cap rock of natural gas reservoirs.

3. Sample and Experimental Method

The experimental samples were obtained from drilling cores of the MT1 and SC1 Wells (well locations are shown in Figure 1a) situated in the central and eastern regions of Ordos Basin. There are 12 cores in total, located in the Ordovician Majiagou Formation, with depths ranging from 2471.54 m to 3541.55 m. The rock samples are mainly clayey limestone and limestone dolomite.

The primary test methods include petrographic conservation, laser Raman spectroscopy, and fluid inclusion microthermometry. The above experiments were completed in the State Key Laboratory of Continental Dynamics, Northwest University, Xi'an, China.

The core samples were made into 0.1–0.2 mm thick double polished fluid inclusion lenses. The classification, size, distribution, and fluorescence characteristics of the inclu-

sions were determined using a standard Leica petrographic microscope under orthogonal polarizer and fluorescence irradiation.

Laser Raman investigations on fluid inclusions were conducted utilizing the LabRAM Odyssey model laser confocal Raman spectrometer manufactured by HORIBA, Kyoto, Japan. The Raman displacement was calibrated using monocrystalline silicon prior to the test, with an error margin of ± 0.5 cm^{-1}. The laser wavelength was 532 nm, the power was 100 mW, the spot size was 1 μm, and the composition of the larger inclusion was ascertained. In the laser Raman results, due to factors such as fluorescence effects, the background values of some individual samples are relatively high. We use LabSpec 6 to perform polynomial fitting on them to eliminate the influence of the background.

The homogenization temperature of fluid inclusions indicates the paleogeothermal temperature during the hydrocarbon accumulation stages, hence facilitating the determination of the accumulation time and thermal evolution history of the hydrocarbon reservoir [29]. The complicated structure of hydrocarbon inclusions can lead to migration, recrystallization, and changes in chemical composition under intricate geological settings, resulting in a difference between the homogenization temperature and the original temperature. Aqueous inclusions are uncomplicated and stable, effectively representing the thermal dynamics of the reservoir [30]. In this study, aqueous inclusions, which belong to the same fluid inclusions assemblage (FIA) as hydrocarbon inclusions, were selected for microthermometry [31,32]. The homogenization temperature of fluid inclusions is the temperature at which the gas phase and liquid phase transform into a single homogeneous liquid phase. First, the liquid phase in the fluid inclusions is frozen, and then it is gradually heated. During this process, it goes through solid, liquid, and gas states. The temperature at which ice melts and the maximum melting temperature are then recorded. The specific operations are as follows: The Linkam THMSG600 cold–hot platform, Linkam Scientific Instruments, Surrey, UK, was used to measure the temperature of fluid inclusion. Artificial pure H_2O inclusion and a 25% H_2O-CO_2 fluid inclusion (international standard sample) were utilized for calibration prior to the experiment. The fluid inclusion is initially chilled to −120 °C at a rate of 5 °C/min for a duration of 1 min until it is entirely frozen. The temperature was subsequently elevated at a rate of 5 °C/min to −60 °C for 1 min, after which the pace was decreased to 0.5 °C/min, reaching –56.6 °C and maintained for 1 min. Subsequently, modify the rate to 3 °C/min and elevate the temperature to −10 °C, maintaining this for 1 min, before increasing the temperature to 10 °C at a rate of 1 °C/min. The temperature was elevated to 100 °C at a rate of 5 °C/min and was thereafter regulated to 3 °C/min for uniformity, and decreased as it neared the phase transition point, with the critical point temperature documented.

4. Results

4.1. Petrological Characteristics

The diagenetic process underpins the research of fluid inclusions. Prior research indicates that the diagenetic process of the Lower Paleozoic carbonate reservoirs in the study area can be categorized into multiple stages: quasi-syngenetic rock, early diagenetic rock, superdiagenetic rock, and middle–late diagenetic rock (Figure 2). The diagenesis of the Ordovician strata during deposition primarily encompasses dolomitization (Figure 3f), compaction and pressure dissolution (Figure 3e), fracturation (Figure 3c), dissolution (Figure 3b), and cementation (Figure 3g) [33]. During the initial diagenetic phase, the strata experienced fracturing because of compaction forces. In the syngenetic environment, annular and extensive cementation occurred on the sediment surface, alongside quasi-syngenetic dolomitization and exhumations. In the epigenetic stage, the strata were subjected to weathering and denudation, mainly by epigenetic dissolution and fracture. In the middle to deep

burial diagenetic period, the overlying formation pressure becomes the main influencing factor in the diagenetic process, and the formation is mainly subjected to compaction and pressure dissolution.

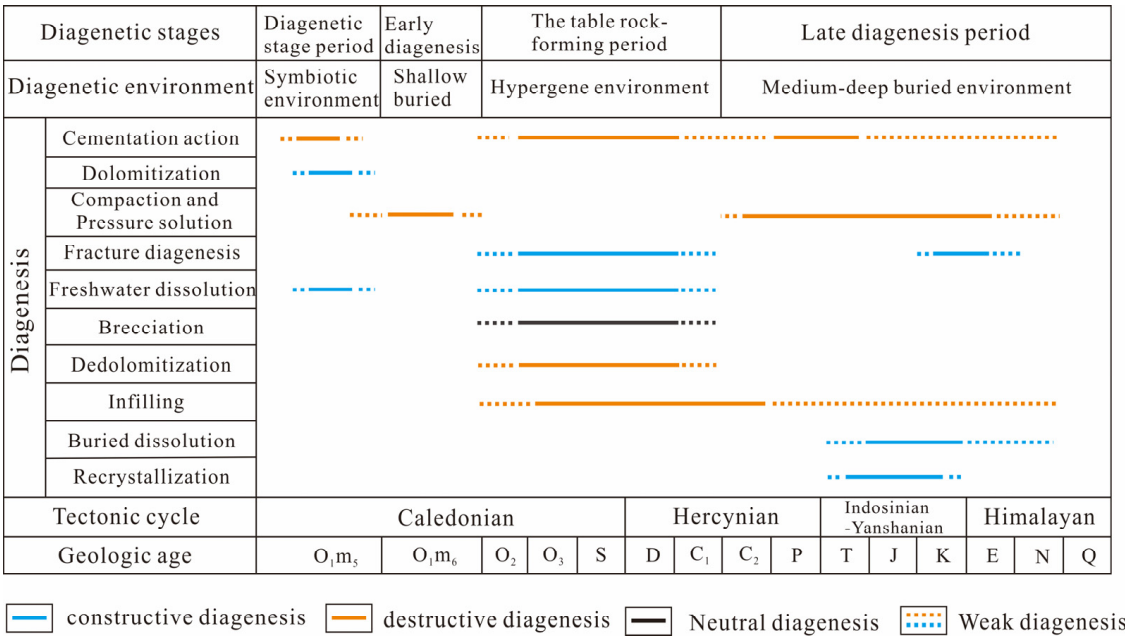

Figure 2. Diagenetic sequence of Ordovician Majiagou Formation reservoir in Ordos Basin (modified from Yu et al., 2012 [34]). O_1m_5: Early Ordovician; O_2: Middle Ordovician; O_3: Late Ordovician; S: Silurian; D: Devonian; C_1: Early Carboniferous; C_2: Late Carboniferous; P: Permian; T: Triassic; J: Jurassic; K: Cretaceous; E: Paleogene; N: Neogene; and Q: Quaternary. Constructive diagenesis refers to the action that occurs in the process of sediment burial and compaction, which is conducive to rock formation or strengthening rock structure. Destructive diagenesis refers to the process in which the physical or chemical properties of sediments are adversely changed and the stability of rocks is reduced due to changes in pressure, temperature, or chemical action during the burial of sediments. Neutral diagenesis refers to the process in which, during diagenesis, the relevant actions do not significantly demonstrate either constructive or destructive effects on the rock.

In the area that was studied, the Ordovician Majiagou Formation reservoir space is mostly made up of naturally microfractures and dissolved pores that are mostly filled with calcite [35]. Numerous cross-shaped and irregular tension cracks, filled with calcite, formed veins in the samples (Figure 3). During the Caledonian tectonic movement, the basin underwent uniform uplift, which in turn led to the Majiagou Formation experiencing weathering, denudation, and dissolution. This process resulted in numerous dissolution cavities filled with calcite. During the Indosinian and Yanshanian, the strata underwent compression, resulting in many fractures, some of which intersected early dissolution cavities and became filled with calcite. The observation and analysis of carbonate samples from Majiagou Formation show that dissolution and fracture are more active.

4.2. Fluid Inclusion

Fluid inclusion refers to an independent closed system in which fluids are trapped by mineral lattice defects and have clear boundaries with minerals during geological processes. Fluid inclusion, as a closed system, encapsulates the temperature, pressure, and composition of the intermediate fluid during hydrocarbon migration and accumulation. We can use this information to determine the paleotemperature and reconstruct the thermal history of the basin, providing a direct and efficient method for analyzing the history of hydrocarbon charging [36–38]. This work seeks to delineate the oil and gas accumulation stages of

Majiagou Formation reservoir in the study region through an analysis of the microscopic characteristics of fluid inclusions, laser Raman spectral properties, and homogenization temperatures.

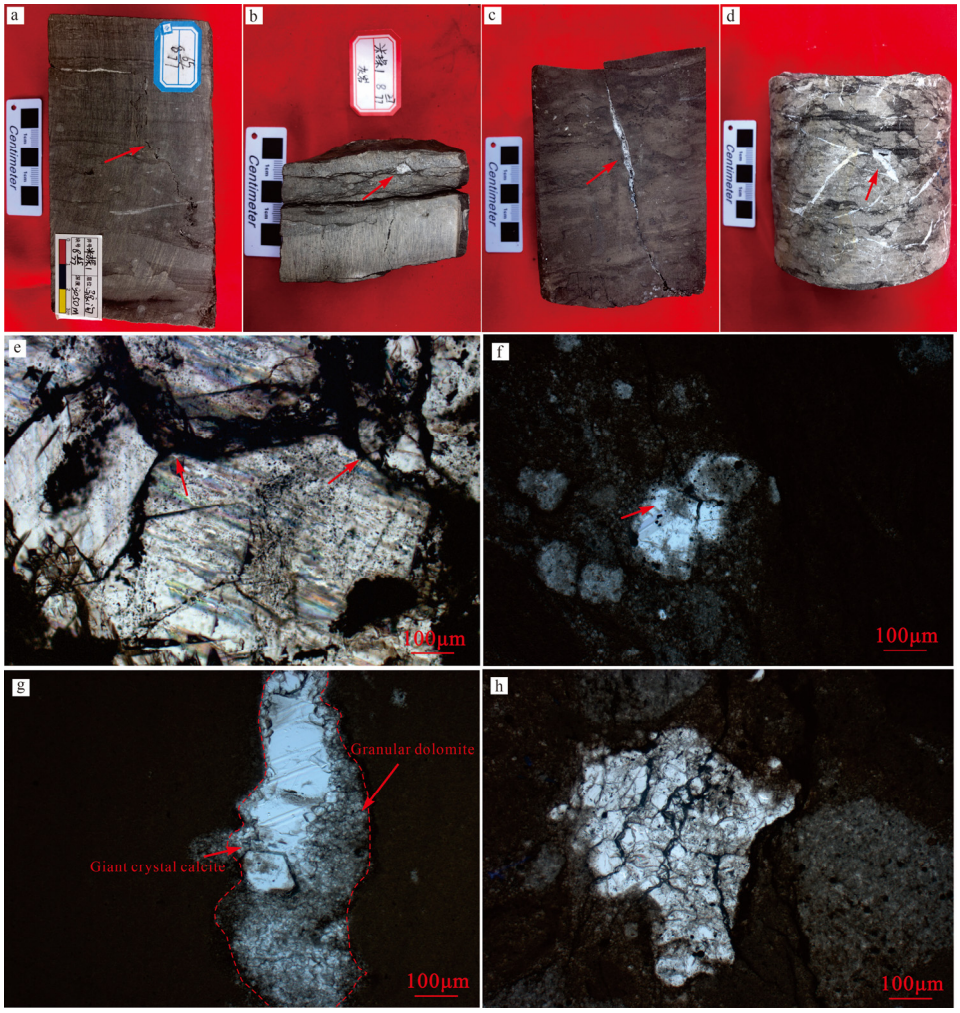

Figure 3. Petrological characteristics of Majiagou Formation in central and eastern Ordos Basin: (**a**) limestone, fissure filled calcite, MT1 well, Ma 4; (**b**) bituminous lamellar limestone, the calcite filling in the solution hole is cut through the fracture, MT1 well, Ma 4; (**c**) argillaceous limestone, high angle fractures filled with calcite, MT1 well, Ma 4; (**d**) laminated limestone, late irregular cracks cut early dissolved pores, filled with calcite, MT1 well, Ma 4; (**e**) single polarizer (5×), bituminous lamellar limestone, compaction and pressure dissolution, MT1 well, 2646.57 m, Ma 4; (**f**) single polarizer (5×), argillaceous limestone, calcite dolomitization, SC1 well, 3475 m Ma 5; (**g**) single polarizer (5×), argillaceous limestone, granular dolomite and giant calcite cemented filling, SC1 well, 3550 m, Ma 5; (**h**) single polarizer (5×), argillaceous limestone, dissolution cavity filled with calcite, SC1 well, 3475 m, Ma 5.

4.2.1. Characteristics of Fluid Inclusion

According to the sample's micropetrographic analysis (Figure 4), the fluid inclusions in the calcite of the Ordovician Majiagou Formation fall into the following categories:

- Gas–liquid hydrocarbon inclusions, measuring between 2 and 6 μm, are devoid of color and transparent. They predominantly manifest in a bead-like arrangement within cracks and dissolved cave containing calcite, displaying round, elliptical, and irregular forms. They exhibit a blue appearance under fluorescence (Figure 4a–c).
- Gaseous hydrocarbon inclusions, measuring 2 to 6 μm, are colorless and clear with dark brown margins, predominantly exhibiting round and irregular forms. We find

them isolated within late sparite calcite, where they occur in relatively low abundance and lack fluorescence (Figure 4d1).

- The asphalt inclusions, measuring between 3 and 8 μm, appear dark brown or black under polarized light and are found irregularly in isolation, lacking fluorescence (Figure 4d2,e).
- Under a polarized microscope, the gas–liquid two-phase saline inclusions appear gray, zonally dispersed in cracks, and filled with calcite. They range in size from 4 to 12 μm and are predominantly elliptical, long columnar, or irregular in shape, lacking fluorescence and exhibiting low abundance (Figure 4g).
- The liquid hydrocarbon inclusions, measuring between 2 and 8 μm, exhibit a brown hue under a single polarizer and are arranged in a beaded pattern within the calcite-filled fractures, appearing elliptical and elongated, accompanied by a blue fluorescence (Figure 4h,i).

As oil and gas evolve from low maturity to overmaturity, the fluorescence of inclusions transitions from red, yellow-green, and blue-white to colorless. The fluorescent color and brightness of fluid inclusions can be utilized to differentiate the characteristics and evolutionary stages of oil and gas to a certain degree [39]. Based on the microscopic morphology and fluorescence coloration of the inclusions, they can be categorized into two stages: The first stage is mostly made up of gas–liquid inclusions that contain liquid hydrocarbons and show blue fluorescence. This shows that oil entered into the reservoir early on in its formation. The second stage mainly consists of asphalt inclusions and gas–liquid inclusions containing gaseous hydrocarbons, which correspond to the gaseous hydrocarbons entering the reservoir in the late stage of reservoir formation. The bitumen and hydrocarbon inclusions in Majiagou Formation within the study area substantiate the presence of an ancient reservoir, indicating that the Majiagou Formation reservoir has experienced crude oil charging and thermal cracking, thereby partially demonstrating the conversion of the ancient reservoir into a natural gas reservoir [13].

4.2.2. Fluid Inclusion Composition Analysis

Laser Raman spectroscopy is a crucial technique for the in situ characterization of inclusions without causing harm. Its principle is the scattering of incident light. When a laser beam hits the fluid inclusion sample, most of the light undergoes elastic scattering (Rayleigh scattering), but a small portion is inelastic scattering (Raman scattering). The wavelength of this inelastic scattered light changes, which is related to the molecular vibration or rotational energy level of the substance. The scattering of laser light produces Raman signals related to the molecular characteristics of the fluid, which can provide a variety of information about the fluid [40]. Throughout the migration of oil and gas, the composition of biological matter undergoes continual alteration. Analyzing the variations in fluid inclusion composition at distinct stages allows for the determination of the period of oil and gas migration [41,42].

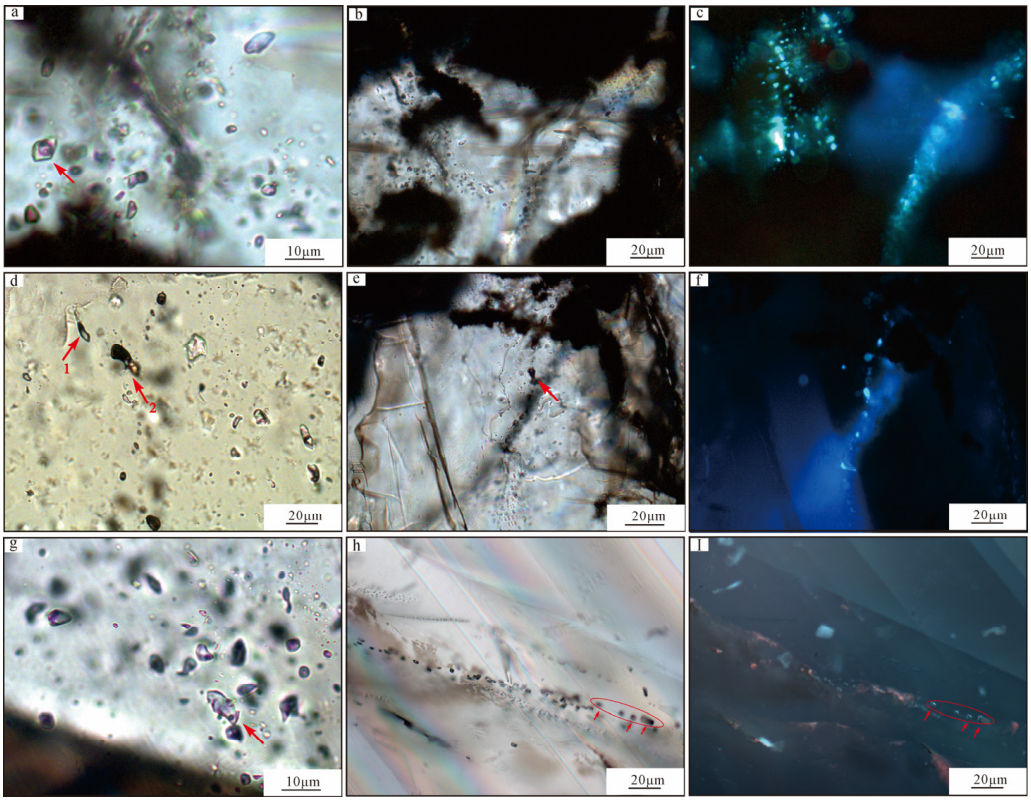

Figure 4. Petrographic characteristics of fluid inclusions in Majiagou Formation, Central and eastern Ordos Basin: (**a**) single polarizer (50×), gas–liquid hydrocarbon inclusions, MT1, depth 2646 m, Ma 4; (**b**) single polarizer (20×), containing liquid hydrocarbon inclusions, MT1, depth 2646 m, (**c**) same view as (**b**), but fluorescing blue under fluorescent irradiation; (**d**) single polarizer (20×), 1. gaseous hydrocarbon inclusion, 2. asphalt inclusion, MT1, depth 2646.57 m, Ma 4; (**e**) single polarizer (20×), asphalt inclusion, MT1, depth 2654.4 m, Ma 4; (**f**) same view as (**e**), but fluorescing blue under fluorescent irradiation; (**g**) single polarizer (50×), gas–liquid two-phase saline inclusions, MT1, depth 2471 m, Ma 4; (**h**) single polarizer (20×), liquid hydrocarbon coating, SC1, depth 3480 m, Ma 5; (**i**) same field of view as (**h**), but fluorescing blue under fluorescent irradiation.

We used laser Raman spectroscopy to look at fluid inclusions from Majiagou Formation of the Early Paleozoic in the study area (Figure 5). The spectra showed that the fluids had bituminous peaks D (peak is about 1350 cm^{-1}, which represents the C-C stretching vibration in the aromatic ring and is an important sign for identifying hydrocarbons) and G (peak values 1573 to 1613 cm^{-1}, the annular C-H bending vibration peak, which mainly represents the presence of aromatic rings and often appears in asphalt samples) [43]. It also contains CH_4 (peak 2909 cm^{-1}), highly saturated hydrocarbons (peak 2700–2970 cm^{-1}) and other components. The reservoir includes bitumen, a byproduct of oil cracking, indicating that the Majiagou Formation in the examined region underwent initial oil charging.

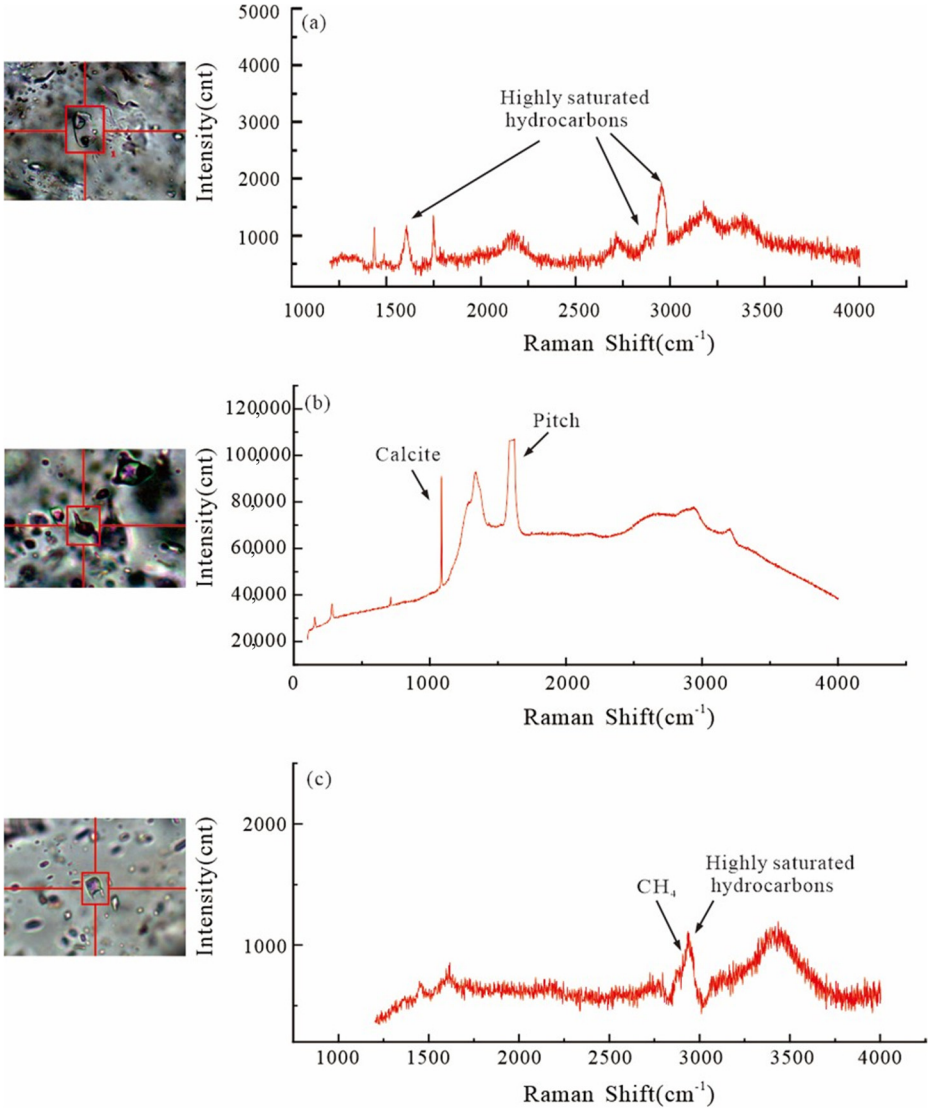

Figure 5. Laser Raman spectra of reservoir fluid inclusions in the Ordovician Majiagou Formation, Ordos Basin: (**a**) MT1 well, depth 2642.57 m, Ma 4; (**b**) MT1 well, depth 2642.57 m, Ma 4; (**c**) MT1 well, depth 3042.8 m, Ma 4.

4.2.3. Microthermometry

The results show that the homogenization temperature (Th) of fluid inclusions in Majiagou Formation reservoir is between 70 °C and 210 °C (Table 1). There are two uniform peak temperature ranges (105–115 °C and 165–175 °C) in the temperature measurement results of the MT1 inclusion (Figure 6a). The inclusion temperature measurement of SC1 reveals two primary peaks (85–95 °C) and (175–185 °C) and a secondary peak (105–115 °C) (Figure 6b). The Th of inclusions in the research area exhibits a continuous distribution with two distinct peak intervals, suggesting that the Majiagou Formation reservoir has undergone a minimum of two stages of oil and gas charging events. Most of the low-temperature inclusions are inclusions containing liquid hydrocarbons with fluorescence display, corresponding to the process of formation and migration of early liquid hydrocarbons into the reservoir. Most of the high-temperature fluid inclusions are gaseous hydrocarbon inclusions without fluorescence display, which indicates the natural gas reservoir-forming period [43,44].

Table 1. Temperature measurement results of fluid inclusions in Ordovician in the Ordos Basin.

Sample ID	Depth/m	Lithology	Occurrence	Types of Fluid Inclusions	Number	T (°C)	Tm (°C)
MT1-1	3050	limestone	Vein filling	Aqueous inclusions associated with hydrocarbon inclusions	6	165–215	-
MT1-1	3050	limestone	Vein filling	Aqueous inclusions	4	131–150	−3.5~−4.5
MT1-1	3050	limestone	Vein filling	Aqueous inclusions associated with liquid hydrocarbon inclusions	4	106–140	-
MT1-13	2654.4	limestone	Vein filling	Aqueous inclusions associated with hydrocarbon inclusions	6	162–210	−7.5~−7.9
MT1-13	2654.4	limestone	Vein filling	Aqueous inclusions associated with liquid hydrocarbon inclusions	10	98–116	−2.9~−4.2
MT1-13	2654.4	limestone	Vein filling	Aqueous inclusions associated with liquid hydrocarbon inclusions	8	110–146	-
MT1-19	2642.57	limestone	Vein, pore filling	Aqueous inclusions associated with hydrocarbon inclusions	10	160–208	−6.9~−12.0
MT1-19	2642.57	limestone	Vein, pore filling	Aqueous inclusions associated with liquid hydrocarbon inclusions	10	101–140	−2.0~−4.1
MT1-19	2642.57	limestone	Vein, pore filling	Aqueous inclusions associated with bitumen inclusion	12	154–196	−4.4~−8.0
MT1-19	2642.57	limestone	Vein, pore filling	Aqueous inclusions associated with hydrocarbon inclusions	8	158–195	-
MT1-32	2471.24	dolomite	Pore filling	Aqueous inclusions associated with liquid hydrocarbon inclusions	7	75–130	−3.5~−4.0
MT1-32	2471.24	dolomite	Pore filling	Aqueous inclusions	12	127–175	−3.1~−4.9
SC-10	3550.05	limestone	Pore filling	Aqueous inclusions	15	140–162	−4.1
SC-10	3550.05	limestone	Pore filling	Aqueous inclusions associated with liquid hydrocarbon inclusions	8	83–102	-
SC-15	3480	limestone	Vein filling	Aqueous inclusions associated with hydrocarbon inclusions	28	163–205	−6.5~−7.0
SC-15	3480	limestone	Vein filling	Aqueous inclusions associated with liquid hydrocarbon inclusions	17	85–101	−2.2~−3.2
SC-18	3475	limestone	Pore filling	Aqueous inclusions associated with hydrocarbon inclusions	21	108–180	−5.2~−7.9
SC-25	3458	limestone	Pore filling	Aqueous inclusions associated with bitumen inclusion	18	160–190	−7.1~−7.5
SC-25	3458	limestone	Pore filling	Aqueous inclusions associated with liquid hydrocarbon inclusions	6	110–148	−3.8
SC-32	3435	dolomite	Pore filling	Aqueous inclusions associated with bitumen inclusion	9	90–193	-

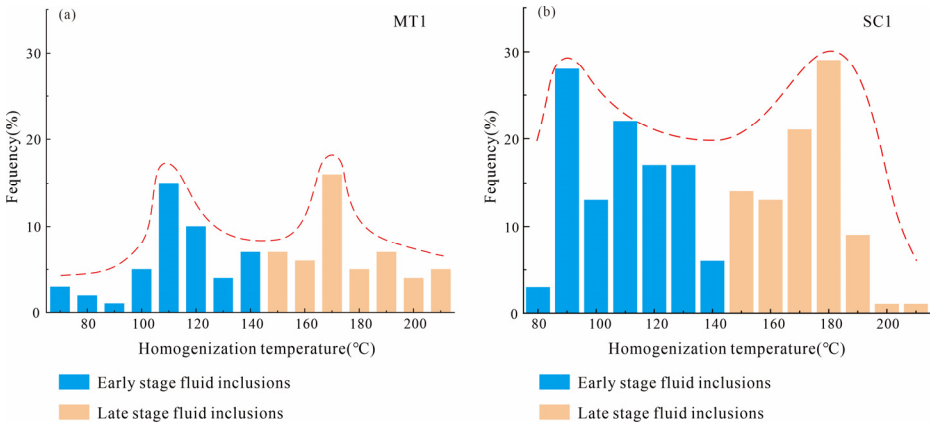

Figure 6. Homogenization temperature histogram of fluid inclusions in the study area: (**a**) Well MT1; (**b**)Well SC1.

Salinity can reflect changes in the sedimentary environment and is an important parameter of fluid inclusions. The salinity and density can be determined based on the homogenization and ice melting temperatures (T_m) of inclusions. The T_m of samples from the Ordovician Majiagou Formation in the research area ranges from −12 °C to −0.8 °C, while their salinity varies from 1.40 to 15.96 wt% NaCl equivalent, as per the saline-T_m conversion chart of Steele-MacInnis [45]. The sample contains two inclusions with varying

salinities (Figure 7). The salinity of the first stage inclusions ranges from 1.40 to 7.17 wt% NaCl equivalent, while the second stage ranges from 6.45 to 15.96 wt% NaCl equivalent. The inclusions in the research area exhibit low overall salinity, categorizing them under a low salinity system. The density range is limited, spanning from 0.920 to 1.002 g/cm^3 (Figure 8). The salinity trend reflects that the salinity of early inclusions is lower. Late inclusions with high salinity indicate that the diagenetic environment changes from shallow to deep, and the fluid evolves from low salinity to high salinity.

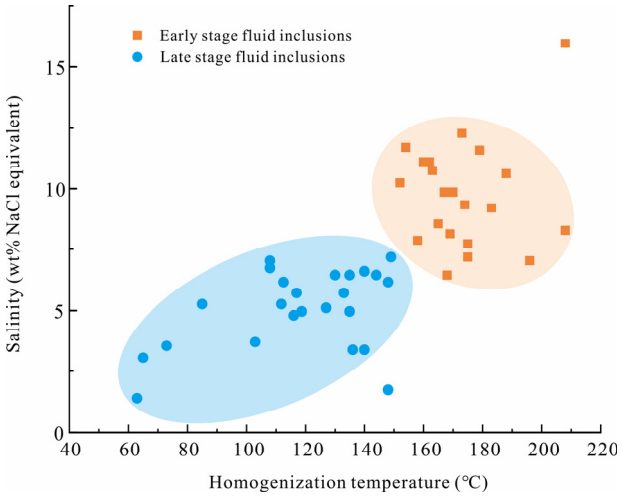

Figure 7. Homogenization temperature–salinity relationship diagram of fluid inclusions in the study area.

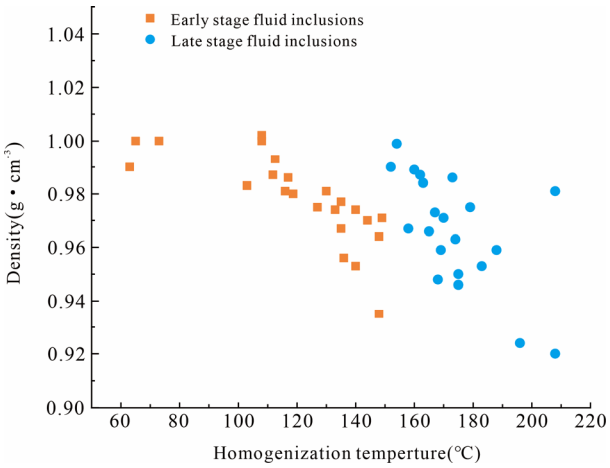

Figure 8. Homogenization temperature–density relationship diagram of fluid inclusions in the study area.

Variations in the salinity of the inclusions may serve as a reliable indicator of the fluid source and the sealing of the trap [36]. The deep trap is effectively sealed, undisturbed by tectonic activity, and the fluid environment remains relatively steady. The salinity of fluids in a closed environment is generally higher than that in an open environment. The decrease in the salinity of the early to late fluid inclusions may be due to the relatively high salinity of the formation water in the early period of crude oil charging. In the late natural gas charging period, fresh fluid injections resulted in a decrease in the salinity of fluid inclusions.

5. Discussion

5.1. History of Thermal Evolution

The phase state, migration, and accumulation of oil and gas are influenced by the thermal evolution history of the basin, and the changes in the basin's tectonic thermal evolution will lead to changes in the accumulation period. The burial and thermal evolution histories can significantly enhance the precision of the accumulation period analysis [46]. The reservoir-forming eras of the Majiagou Formation can be deeply studied based on the thermal history reconstruction of the basin and the characteristics of fluid inclusions.

The Ordovician system of the basin experienced a process of first warming and then cooling. The heat flow value of the basin ranged from 55 to 60 mW/m² over the Early Paleozoic to Middle Jurassic, subsequently exhibiting a progressive increase. During the Early Cretaceous period, the lithosphere's thickness diminished, and tectonic thermal events transpired in the basin, with heat flow values peaking at around 90 mW/m² in the late Early Cretaceous. The thermal event persisted for almost 70 Ma, with the heat flow value consistently above 70 mW/m². Thereafter, the heat flow value progressively diminished, with the current basin heat flow value approximating 62 mW/m^2 [15,47].

Significant disparities exist in the extent of Ordovician thermal evolution throughout various regions of the Ordos Basin. The thermal evolution degree at the top of the Ordovician basin (Figure 9) is generally higher in the south and lower in the north and tends to decrease from the interior of the basin to the periphery of the basin. Vitrinite reflectance (*Ro*) at the top of the Ordovician is generally higher in the basin, and the overall value is greater than 2.0%. There are abnormally high values in the southern part of the basin, and *Ro* can reach more than 3.0%. The eastern section of the basin experienced significant compression and uplift due to the Yanshanian tectonic action near the conclusion of the Late Jurassic period. During the early phase of the Cretaceous period, the eastern strata were deposited at shallow depths and distanced from the thermal anomaly center located in the southern basin, leading to a reduced level of thermal evolution in the eastern region compared to the interior.

We used PetroMod basin simulation software to recover the thermal evolution history of the basin using the Easy% *Ro* model. The thorough examination of the thermochronological evolution of the basin indicates that well SC1 (Figure 10) in the central basin was deposited during the Middle–Late Ordovician; however, at this time, the formation depth was shallow, the formation temperature was low, and the source rock was in an immature state. Since then, the formation has undergone uplift and denudation for about 150 Ma. The strata commenced settling once more from the Permian, and throughout the Late Triassic to Early–Middle Jurassic, the source rocks attained the oil generation threshold and entered the primary oil generation stage. During the Yanshanian Movement, numerous tectonic fissures formed in the strata due to compressive forces, providing pathways and reservoirs for hydrocarbon migration. Following persistent subsidence, the burial depth of the Ordovician strata attained its zenith in the Early Cretaceous, reaching 5200 m. Due to the maximum paleothermal conditions of the Early Cretaceous, the temperature of the Ordovician strata peaked during this period, exceeding 195 °C. The vitrinite reflectance reached a maximum of 2.4% in the Early Cretaceous, and it was at the stage of dry gas generation.

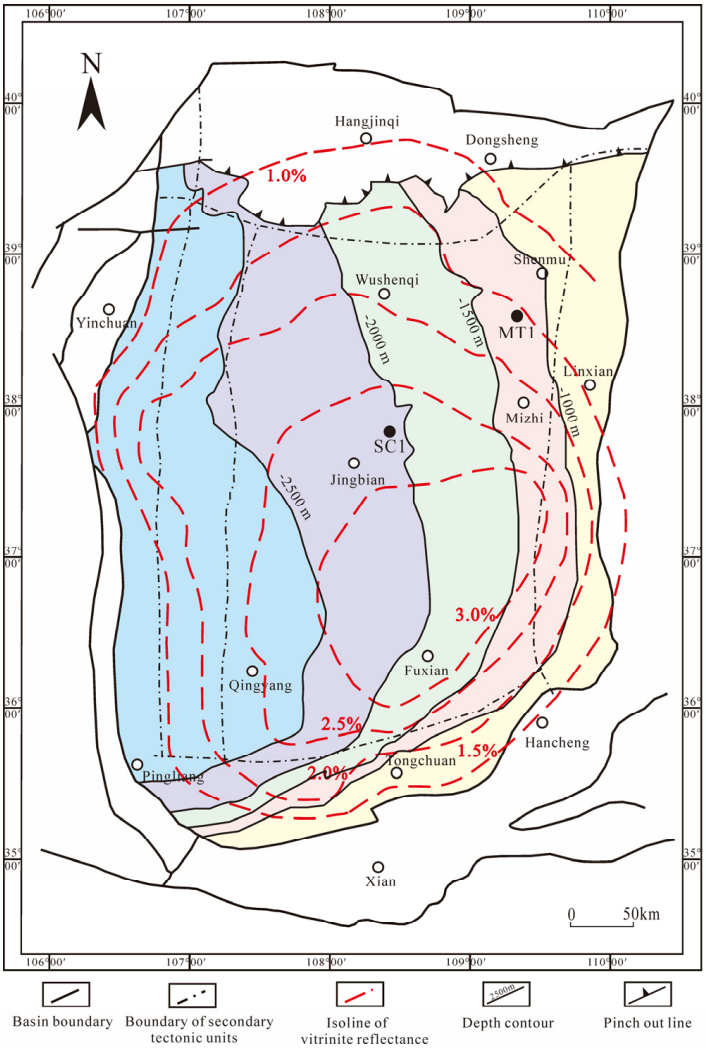

Figure 9. Distribution map of vitrinite reflectance at the top of the Ordovician strata in the Ordos Basin [3,48].

The simulation of the thermal evolution history of well MT1 (Figure 11) in the eastern part of the basin shows that the Lower Paleozoic strata settled rapidly in the Early and Middle Ordovician, with the depth of the strata being up to 2000 m, but the basin heat flow value is low and the formation temperature is low. With the continuous subsidence of strata, the formation temperature gradually increased, and the Lower Paleozoic strata entered the main oil-generating stage in the Late Triassic and Early Jurassic. After that, the strata continued to be buried deeper, reaching a maximum depth of about 4300 m at the end of the Early Cretaceous. In addition, the geothermal heat flow increased significantly in the Middle Jurassic and Early Cretaceous, so the temperature and thermal evolution of the strata reached the highest value at the end of the Early Cretaceous, with an *Ro* about 1.66%, which was the main stage of natural gas charging.

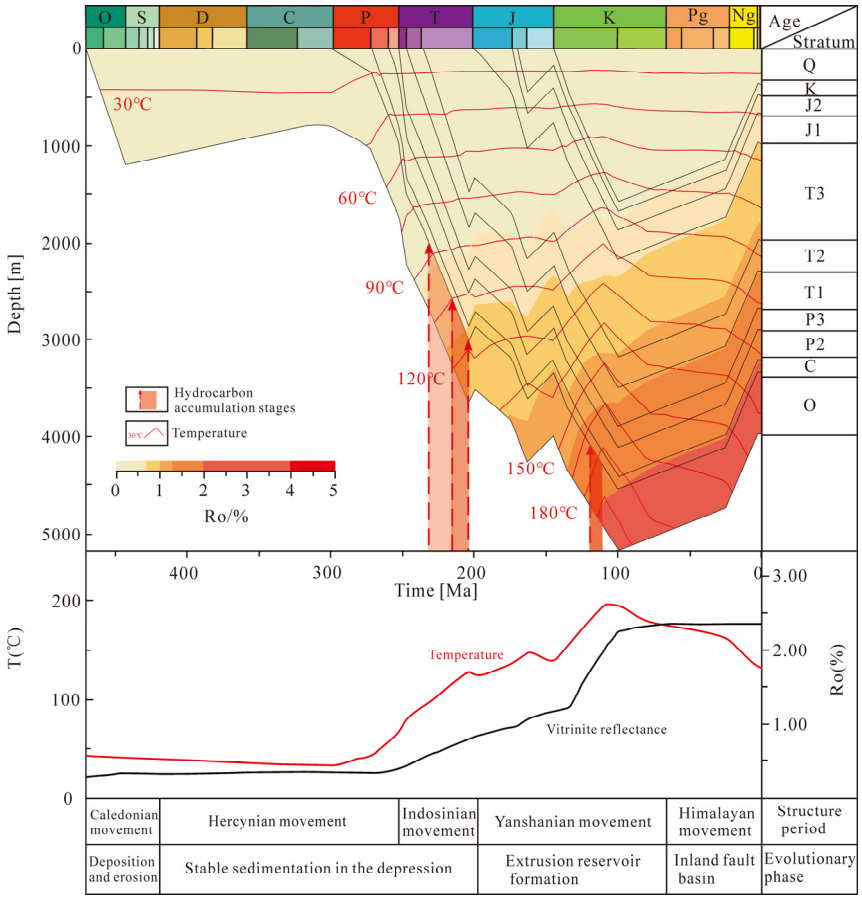

Figure 10. Recovery of thermal evolution history and accumulation period of Ordovician in well SC1. Stratum: O: Ordovician; C: Carboniferous; P2: Middle Permian; P3: Upper Permian; T1: Lower Triassic; T2: Middle Triassic; T3: Upper Triassic; J1: Lower Jurassic; J2: Middle Jurassic; K: Cretaceous; Q: Quaternary. Age: O: Ordovician; S: Silurian; D: Devonian; C: Carboniferous; P: Permian; T: Triassic; J: Jurassic; K: Cretaceous; Pg: Paleogene; N: Neogene.

5.2. Comprehensive Analysis of Accumulation Stages

Based on the types, occurrences, homogenization temperatures, and ice melting temperatures of fluid inclusions, the inclusion assemblages of the Ordovician Majiagou reservoir in the study area can be divided into two types: (1) Dominated by liquid hydrocarbon inclusions and aqueous inclusions, these fluid inclusions are mostly developed in the sparite calcite of dissolution pores and cavities. Among them, the liquid hydrocarbon inclusions exhibit blue fluorescence, and the homogenization temperatures of the co-trapped aqueous inclusions mainly range from 100 °C to 120 °C. During the trapping period of these fluid inclusions, the Lower Paleozoic source rocks had entered the oil generation threshold. (2) The inclusion assemblage is composed of gaseous hydrocarbon inclusions, bitumen inclusions, and associated aqueous inclusions, which mainly exist in calcite veins and sparite calcite. The bitumen inclusions show blue-white fluorescence, while the gaseous hydrocarbon inclusions show no fluorescence. The temperatures of the associated aqueous inclusions mainly range from 160 to 180. When these fluid inclusions were trapped, the Lower Paleozoic source rocks had entered the high-maturity to over-maturity stage, and the paleo-oil reservoirs underwent high-temperature cracking, generating a large amount of gaseous hydrocarbons.

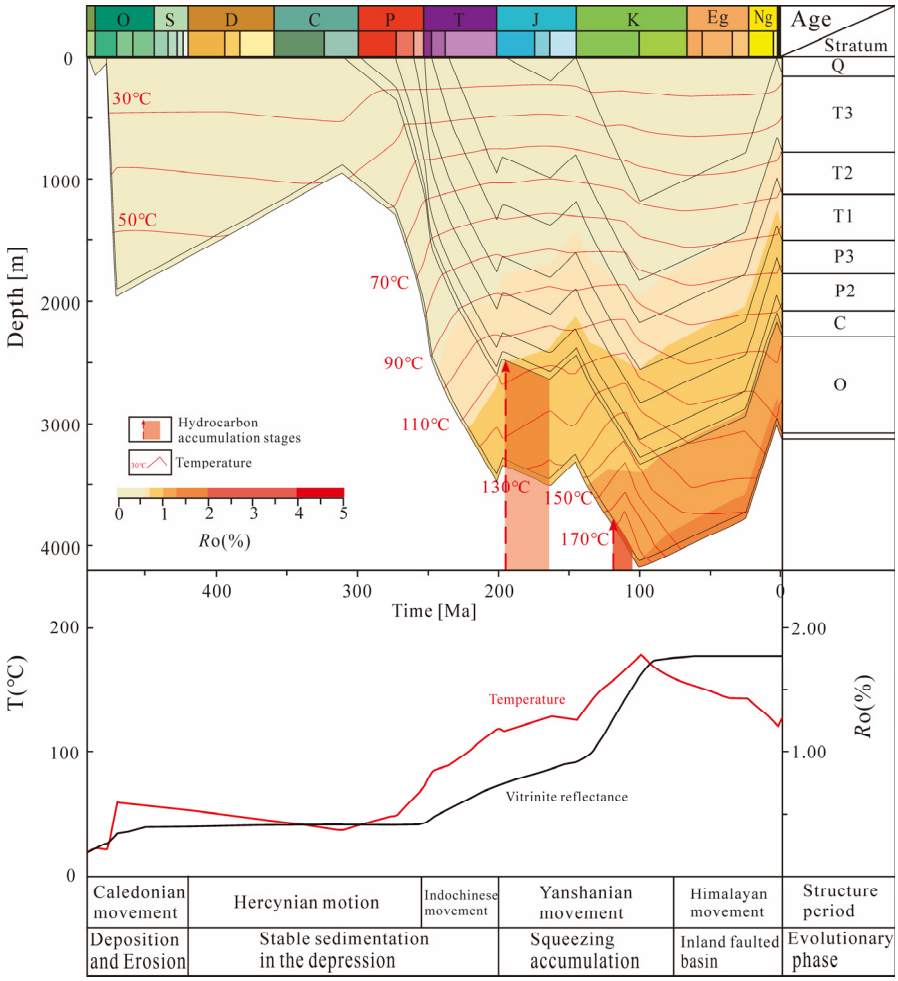

Figure 11. Recovery of thermal evolution history and accumulation period of Ordovician in well MT1. Stratum: O: Ordovician; C: Carboniferous; P2: Middle Permian; P3: Upper Permian; T1: Lower Triassic; T2: Middle Triassic; T3: Upper Triassic; Q: Quaternary. Age: O: Ordovician; S: Silurian; D: Devonian; C: Carboniferous; P: Permian; T: Triassic; J: Jurassic; K: Cretaceous; Pg: Paleogene; N: Neogene.

Based on previous research and a close look at the inclusion of homogenization temperature and the thermal evolution history of the basin, it was found that the Majiagou reservoir in the central and eastern Ordos Basin mostly went through two periods of oil and gas charging. The maximum uniform temperature values in the Shenmu region of the eastern basin ranged from 105 °C to 115 °C and 165 °C to 175 °C, respectively. During the Early–Middle Jurassic period (about 196 Ma to 164 Ma), the source rock commenced the oil-generating stage, and the reservoir mostly experienced oil influx. During the Late–Early Cretaceous (about 110 Ma to 101 Ma), the temperature of the Ordovician Formation peaked, entering the gas generation stage, characterized by the accumulation of natural gas. The maximum temperature of the inclusions in the Yan'an region ranges from 120 °C to 140 °C and 160 °C to 170 °C, indicating that the initial stage of oil charging transpired during the Middle–Late Jurassic, while the subsequent stage of natural gas charging occurred in the Late–Early Cretaceous [49]. The maximum temperature of inclusions in the Wuqi area inside the central basin varies between 110 °C to 130 °C and 160 °C to 170 °C. The initial stage of oil and gas injection occurred from the Late Triassic to the Middle Jurassic (210–165 Ma), whereas the subsequent stage transpired from the Early Cretaceous (123–97 Ma) [50]. The temperature measurement results of inclusions in the Jingbian area indicate two primary peaks at 85 to 95 °C and 175 to 185 °C, respectively. The reservoirs

commenced oil and gas charging during the Late Triassic period (about 231 to 203 Ma) and reached the zenith of natural gas charging in the Early Cretaceous period (about 121 to 112 Ma). They are associated with the late Indosinian and Yanshan Movements. The period of oil and gas accumulation in the Majiagou reservoir aligns approximately with the timing of thermal events in the basin [46], specifically during the late Early Cretaceous, influenced by thermal anomalies. During this time, the oil present in the reservoir experienced cracking, which led to the formation of bitumen and natural gas, thus indicating the onset of an era characterized by substantial natural gas accumulation.

Upon comparing the reservoir-charging duration of Majiagou Formation across various regions of the central and eastern basins, it is observed that the timing of the two stages of oil and gas charging is generally analogous. However, the oil and gas charging in the central basin occurs earlier than in the eastern basin, with the gas charging stage also preceding that of the eastern basin. This phenomenon is influenced by the disparities in thermal evolution and burial history between the basin's interior and its periphery. The strata within the basin are deeply buried and close to the core of the thermal anomaly. This causes them to reach the hydrocarbon generation threshold earlier and enter the gas generation stage, thus making oil and gas charging events occur earlier than those in the basin margin areas.

6. Conclusions

This paper examines the classification of fluid inclusions within the Majiagou Formation reservoir in the central and eastern Ordos Basin, alongside the measurement of homogenization temperature. Additionally, it integrates the simulation of the basin's thermal evolution history to reconstruct the oil and gas accumulation stages of Majiagou Formation reservoir in the study area. The primary conclusions are as follows:

1. The fluid inclusions within the Majiagou Formation reservoir in the central and eastern Ordos Basin are classified into five categories: gas–liquid hydrocarbon inclusions, gaseous hydrocarbon inclusions, gas–liquid saline inclusions, bitumen inclusions, and liquid hydrocarbon inclusions. The inclusions are primarily composed of highly saturated hydrocarbons and CH_4, signifying that hydrocarbon evolution has attained a high maturity level and a substantial quantity of hydrocarbons has been produced.
2. We divide the fluid inclusions in the study area into two stages. The early inclusions mostly consist of gas–liquid hydrocarbon inclusions and liquid hydrocarbon inclusions, exhibiting blue fluorescence. The maximum Th of aqueous inclusions varies from 85 °C to 95 °C in the central basin and from 105 °C to 115 °C in the eastern basin. The inclusions in the second stage are mostly gaseous hydrocarbons, with a small amount of asphalt also present. They do not fluoresce in a noticeable way. The maximum homogenization temperature varies from 175 °C to 185 °C in the central basin and from 165 °C to 175 °C in the eastern basin.
3. The Majiagou Formation reservoir in the study region typically experienced two stages of oil and gas charge. The central region of the basin attained the hydrocarbon generation threshold during the Late Triassic (about 231 Ma), marking the oil charging stage. During the middle to late Early Cretaceous period (about 121 to 112 Ma), the primary stage of gas accumulation commenced, coinciding with the accumulation periods of the Indosinian and Yanshan stages. In the eastern region of the basin, oil accumulation transpired during the Early to Middle Jurassic (about 196 to 164 Ma), whereas natural gas accumulation happened in the late Early Cretaceous (about 110 to 101 Ma). The primary accumulation stage aligns with the Yanshan tectonic movement. In comparison to the eastern part of the basin, the central basin has a higher degree of

thermal evolution and oil–gas accumulation started earlier. This is due to the distinct thermal evolution and burial histories in various regions of the basin.

Author Contributions: Conceptualization, Z.R. and Y.L.; methodology, K.Q.; software, G.X.; validation, X.Y., B.X. and J.Y.; investigation, M.J.; resources, Z.R.; data curation, J.L.; writing—original draft preparation, Y.L.; writing—review and editing, Z.R. and J.R.; visualization, H.T. All authors have read and agreed to the published version of the manuscript.

Funding: This research was funded by the PetroChina Changqing Oilfield Company Science and technology Major Projects (ZDZX2021), and PetroChina Changqing Oilfield Company Science and technology Major Projects "Research on Tectonic-Sedimentary Environment, Hydrocarbon Accumulation Conditions and Favorable Exploration Zones in the Deep Strata of Ordos Basin" (2024D1JC06).

Data Availability Statement: The data used to support the findings of this study are available from the first author upon request (first author: Z.L. 202221638@stumail.nwu.edu.cn).

Conflicts of Interest: Author Xinyun Yan was employed by the PetroChina Yumen Oil field Company. Author Beile Xiong was employed by the Yumen Oilfield Branch Huanqing Oil Production Plant. Author Junfeng Ren was employed by the PetroChina Changqing Oil field Company. The remaining authors declare that the research was conducted in the absence of any commercial or financial relationships that could be construed as a potential conflict of interest.

References

1. Ren, Z.L.; Cue, J.P.; Qi, K.; Yang, P.; Liu, X.S.; Zhang, C.L.; Yang, G.L.; Gao, Y.F.; Zhang, Y. New progress in research on theories and methods for reconstruction of deep and ultra-deep thermal evolution history in superimposed basins. *J. Northwest Univ.* **2022**, *52*, 910–929. [CrossRef]
2. Guo, Y.R.; Zhao, Z.Y.; Zhang, Y.Q.; Xu, W.L.; Bao, H.P.; Zhang, Y.L.; Gao, J.R.; Song, W. Development characteristics and new exploration areas of marine source rocks in Ordos Basin. *Acta Pet. Sin.* **2016**, *37*, 939–951, 1068.
3. Yang, P.; Ren, Z.L.; Zhou, R.J.; Cui, J.P.; Qi, K.; Fu, J.H.; Li, J.B.; Liu, X.S.; Li, W.H.; Wang, K.L.; et al. Tectonic evolution and controls on natural gas generation and accumulation in the Ordovician system of the Ordos Basin, North China. *Energy Rep.* **2021**, *7*, 6887–6898. [CrossRef]
4. He, H.Q.; Guo, X.J.; Zhao, Z.Y.; Xi, S.L.; Wang, J.F.; Song, H.; Ren, J.F.; Wu, X.N.; Bi, H. New understandings on gas accumulation and major exploration breakthroughs in subsalt Ma 4 Member of Ordovician Majiagou Formation, Ordos Basin, NW China. *Pet. Explor. Dev. Online* **2022**, *49*, 489–501. [CrossRef]
5. Zhang, W.; Liu, W.H.; Wang, X.F.; Huang, Z.L.; Kong, Q.F.; Luo, H.Y.; Zhang, D.D.; Liu, P.; Chen, X.Y.; Cai, Z.H. Formation Mechanism of Heavy Hydrocarbon Carbon Isotope Anomalies in Natural Gas from Ordovician Marine Carbonate in the Ordos Basin. *J. Mar. Sci. Eng.* **2023**, *11*, 2176. [CrossRef]
6. Yao, J.L.; Bao, H.P.; Ren, J.F.; Sun, L.Y. Exploration of Ordovician Subsalt Natural Gas Reservoirs in Ordos Basin. *China Pet. Explor.* **2015**, *20*, 1–12. [CrossRef]
7. Liu, X.S.; He, J.J.; Wei, L.B.; Liu, B.; Bao, H.P.; Shi, K.B.; Luo, Q.Q.; Wu, C.; Zhao, Q.; Chen, S.R.; et al. Sedimentary characteristics and evolution mechanism of Ordovician pre-salt dolomite reservoirs in the central and eastern Ordos Basin. *Chin. J. Geol.* **2024**, *59*, 637–659.
8. Zhou, J.G.; Zhang, T.; Yu, Z.; Wu, D.X.; Li, C.S.; Ding, Z.C.; Li, W.L.; Liu, Y.X.; Yi, C. Lithofacies paleogeography in the deposition period of the fourth member of the Ordovician Majiagou Formation and its reservoir control effect, Ordos Basin. *China Pet. Explor.* **2022**, *27*, 61–74.
9. Cai, C.F.; Hu, G.Y.; He, H.; Li, J.; Li, J.F.; Wu, Y.S. Geochemical characteristics and origin of natural gas and thermochemical sulphate reduction in Ordovician carbonates in the Ordos Basin, China. *J. Pet. Sci. Eng.* **2005**, *48*, 209–226. [CrossRef]
10. Bao, H.P.; He, D.F.; Wang, Q.P.; Zhang, L.; Zhang, J.W.; Yan, T.; Yan, W. Four main paleouplifts evolution in Ordos Basin and their differences in significance of oil and gas reservoir control. *J. Palaeogeogr.* **2022**, *24*, 951–969. [CrossRef]
11. Mao, D.F.; He, D.F. The characteristics of seismic waves and its geological significance of middepth layers in mideastern Ordos Basin. *Chin. J. Geol.* **2023**, *58*, 165–179.
12. Lou, R.X.; Wang, L.W.; Wang, L.X.; Yang, G.; Wang, J.P.; Liu, C.Y.; Pei, Y.; Zhang, C. Characteristics of fluid inclusions and hydrocarbon accumulation period of Huoshiling-Yingcheng Formations in Wangfu fault depression, Songliao Basin, China. *J. Pet. Sci. Eng.* **2022**, *208*, 109421. [CrossRef]
13. Guo, Y.R.; Fu, J.H.; Wei, X.S.; Xu, W.L.; Sun, L.Y.; Zhao, Z.Y.; Zhang, Y.Q.; Gao, J.R.; Zhang, Y.L. Natural gas accumulation and models in Ordovician carbonates, Ordos Basin, NW China. *Pet. Explor. Dev. Online* **2014**, *41*, 437–448. [CrossRef]

14. Wu, X.L.; Xu, W.L.; Li, R.X.; Li, N.X.; Liu, Q.; Zhao, D.; Zhao, B.S.; Qin, X.L.; Bai, Y. Genesis of hydrogen sulfide in Ordovician Majiagou Formation, mid-eastern Ordos Basin: Evidence from fluid inclusions. *Acta Pet. Sin.* **2022**, *43*, 250–261. [CrossRef]
15. Zou, C.N.; Xie, Z.G.; Li, J.; Zhang, L.; Yang, C.L.; Cui, H.Y.; Wang, X.B.; Guo, Z.Q.; Pan, S.Q. Differences and main controlling factors of large-scale gas accumulations in typical giant carbonate gas fields: A case study on Anyue gas field in the Sichuan Basin and Jingbian gas field in the Ordos Basin. *Oil Gas Geol.* **2023**, *44*, 1–15. [CrossRef]
16. Liu, E.H.; Chen, Z.P.; Wang, Q.C.; Bai, N.; Li, J.; Liao, Y. Genetic types of natural gas from upper & middle assemblage of Majiagou Formation in Jingbian area, Ordos Basin. *J. Xi'an Univ. Sci. Technol.* **2022**, *42*, 324–334. [CrossRef]
17. Li, X.Q.; Hu, G.Y.; Li, J.; Xiong, B.; Mi, J.K.; Tang, Y.J. Characteristics of fluid inclusions in Ordovician carbonate reservoirs in central Ordos Basin and its significance for gas accumulation. *Nat. Gas Geosci.* **2004**, *15*, 120–124.
18. Akhtar, S.; Yang, X.Y.; Pirajno, F. Sandstone type uranium deposits in the Ordos Basin, Northwest China: A case study and an overview. *J. Asian Earth Sci.* **2017**, *146*, 367–382. [CrossRef]
19. Liu, J.; Ren, Z.L.; Yu, Q.; Yan, X.Y.; Qi, K.; Wang, Z.; Lan, H.P.; Jia, M.X.; Liu, Y.Z.; Wu, H. Hydrogeochemistry and genetic mechanisms of the geothermal system in the Xi'an depression of the southern Weihe Basin, China. *Geothermics* **2024**, *122*, 103090. [CrossRef]
20. Peng, H.; Wang, J.L.; Liu, C.Y.; Zhao, H.G.; Huang, L.; Zhao, X.C.; Zhang, S.H.; Liang, C.; Wang, Z.; Silvia, C.; et al. Long-term and multiple stage exhumation of the Ordos Basin, western North China Craton: Insights from seismic reflection, borehole and geochronological data. *Earth-Sci. Rev.* **2023**, *238*, 104349. [CrossRef]
21. Xiao, X.M.; Zhao, B.Q.; Thu, Z.L.; Song, Z.G.; Wilkins, R.W.T. Upper paleozoic petroleum system, Ordos basin, China. *Mar. Pet. Geol.* **2005**, *22*, 945–963. [CrossRef]
22. Yang, M.H.; Li, L.; Zhou, J.; Jia, H.C.; Sun, X.; Qu, X.Y.; Zhou, D.; Gong, T.; Ding, C. Mesozoic structural evolution of the Hangjinqi area in the northern Ordos Basin, North China. *Mar. Pet. Geol.* **2015**, *66*, 695–710. [CrossRef]
23. Krisnabudhi, A.; Sapiie, B.; Riyanto, A.M.; Gunawan, A.; Rizky, F.F. Mesozoic-Cenozoic Stratigraphy and Tectonic Development of the Southern Great Tarakan Basin, Northeast Borneo, Indonesia. *Rud.-Geološko-Naft. Zb.* **2022**, *37*, 123–138. [CrossRef]
24. Yu, C.Y.; Jia, Y.M.; Ren, Z.L.; Wang, Q.C.; Ren, H.J. Geochemical characteristics and genesis of the Ma55 dolomite of Ordovician Majiagou Formation in Daniudi area, Ordos Basin. *Mar. Orig. Pet. Geol.* **2021**, *26*, 375–383. [CrossRef]
25. Xu, W.L.; Li, J.Z.; Liu, X.S.; Li, N.X.; Zhang, C.L.; Zhang, Y.Q.; Fu, L.; Bai, Y.; Huang, Z.L.; Gao, J.R.; et al. Accumulation conditions and exploration directions of Ordovician lower assemblage natural gas, Ordos Basin, NW China. *Pet. Explor. Dev. Online* **2021**, *48*, 641–654. [CrossRef]
26. Katz, B.J.; Everett, M.A. An overview of pre-Devonian petroleum systems–Unique characteristics and elevated risks. *Mar. Pet. Geol.* **2016**, *73*, 492–516. [CrossRef]
27. Du, J.H.; LI, X.B.; Bao, H.P.; Xu, W.L.; Wang, Y.T.; Huang, J.P.; Wang, H.B.; Rong, W.Y.; Wang, J. Geological conditions of natural gas accumulation and new exploration areas in the Mesoproterozoic to Lower Paleozoic of Ordos Basin, NW China. *Pet. Explor. Dev.* **2019**, *46*, 866–882. [CrossRef]
28. Liu, D.; Li, J.; Liu, J.Q.; Zhang, L. Modeling hydrocarbon accumulation based on gas origin and source rock distribution in Paleozoic strata of the Ordos Basin, China. *Int. J. Coal Geol.* **2020**, *225*, 103486. [CrossRef]
29. Zhang, F.Q.; Chen, Z.X.; Zhao, Z.Y.; Gao, J.R.; Fu, L.; Li, C.S.; Zhang, L.X. Hydrocarbon Accumulation Periods in the Upper Paleozoic Strata of the Western Ordos Basin, China, Based on Fluid Inclusions and Basin Modeling. *ACS Omega* **2023**, *8*, 20536–20549. [CrossRef]
30. Shan, Y.P.; Wang, H.J.; Zhang, L.J.; Su, P.H.; Cheng, M.W.; Bai, Z.H. Study on hydrocarbon accumulation periods based on fluid inclusions and diagenetic sequence of the subsalt carbonate reservoirs in the Amu Darya right bank block. *Geofluids* **2022**, *2022*, 2412615. [CrossRef]
31. Goldstein, R.; Reynolds, J. Systematics of fluid inclusions. *SEPM Short Course Notes* **1994**, *31*, 188.
32. Goldstein, R.H. Fluid inclusions in sedimentary and diagenetic systems. *Lithos* **2001**, *55*, 159–193. [CrossRef]
33. Liu, M.J.; Xiong, Y.; Xiong, C.; Liu, Y.; Liu, L.; Xiao, D. Evolution of diagenetic system and its controls on the reservoir quality of pre-salt dolostone: The case of the Lower Ordovician Majiagou Formation in the central Ordos Basin, China. *Mar. Pet. Geol.* **2020**, *122*, 104674. [CrossRef]
34. Yu, Z.; Sun, L.Y.; Wu, X.N.; Yao, X.H.; Ding, Z.C. Characteristics and Controlling Factors of the Middle Array of Ordovician Majiagou Reservoirs to the West of Jingbian Gas Field, Ordos Basin. *Mar. Orig. Pet. Geol.* **2012**, *17*, 49–56. [CrossRef]
35. Mahmoud, H. Automatic characterization and quantitative analysis of seismic facies in naturally fractured reservoir: Case study of Amguid Messaoud field, Algeria. *Min. Miner. Depos.* **2023**, *17*, 42–48. [CrossRef]
36. Guo, Y.C.; Cao, J.; Liu, R.Q.; Wang, H.F.; Zhang, H.Y. Hydrocarbon accumulation and alteration of the Upper Carboniferous Keluke Formation in the eastern Qaidam Basin: Insights from fluid inclusion and basin modeling. *J. Pet. Sci. Eng.* **2022**, *211*, 110116. [CrossRef]
37. Hu, G.Y.; Li, J.; Shan, X.Q.; Han, Z.X. The origin of natural gas and the hydrocarbon charging history of the Yulin gas field in the Ordos Basin, China. *Int. J. Coal Geol.* **2010**, *81*, 381–391. [CrossRef]

38. Li, G.Z.; Qin, Y.; Shen, J.; Wu, M.; Li, C.; Wei, K.H.; Zhu, C. Geochemical characteristics of tight sandstone gas and hydrocarbon charging history of Linxing area in Ordos Basin, China. *J. Pet. Sci. Eng.* **2019**, *177*, 198–207. [CrossRef]
39. George, S.C.; Ruble, T.E.; Dutkiewicz, A.; Eadington, P.J. Assessing the maturity of oil trapped in fluid inclusions using molecular geochemistry data and visually-determined fluorescence colours. *Appl. Geochem.* **2001**, *16*, 451–473. [CrossRef]
40. Frezzotti, M.L.; Tecce, F.; Casagli, A. Raman spectroscopy for fluid inclusion analysis. *J. Geochem. Explor.* **2012**, *112*, 1–20. [CrossRef]
41. Burke, E.A.J. Raman microspectrometry of fluid inclusions. *Lithos* **2001**, *55*, 139–158. [CrossRef]
42. Chen, K.; Zhang, H.R.; Ibrahim, U.K.; Xue, W.Y.; Liu, H.; Guo, A.J. The quantitative assessment of coke morphology based on the Raman spectroscopic characterization of serial petroleum cokes. *Fuel* **2019**, *246*, 60–68. [CrossRef]
43. Zhu, R.J.; Lu, R.X.; Wu, X.L.; Qin, X.L.; Zhao, B.S.; Liu, F.T.; Zhao, D. The Accumulation Characteristics of the Paleozoic Reservoir in the Central-Southern Ordos Basin Recorded by Organic Inclusions. *Geofluids* **2021**, *2021*, 9365364. [CrossRef]
44. Cao, Q.; Wei, X.S.; Chen, Z.X.; Zhao, J.Z.; Tang, M.J. Hydrocarbon Charge History of the Upper Paleozoic, Ordos Basin as Revealed by Fluid Inclusions. *Front. Phys.* **2022**, *10*, 836977. [CrossRef]
45. Steele-MacInnis, M.; Lecumberri-Sanchez, P.; Bodnar, R.J. HokieFlincs_H_2O-NaCl: A Microsoft Excel spreadsheet for interpreting microthermometric data from fluid inclusions based on the PVTX properties of H_2O–NaCl. *Comput. Geosci.* **2012**, *49*, 334–337. [CrossRef]
46. Ren, Z.L.; Liu, L.; Cui, J.P.; Xiao, H.; Gao, S.L. Application of tectonic-thermal evolution history to hydrocarbon accumulation timing in sedimentary basins. *Oil Gas Geol.* **2008**, *29*, 502–506.
47. Qi, K.; Ren, Z.L.; Cui, J.P.; Yu, Q. Meso-Cenozoic lithospheric thermal structure and its significance in the evolution of the lithosphere in the Ordos Basin, WNCC, China. *Int. Geol. Rev.* **2021**, *63*, 2146–2165. [CrossRef]
48. Ren, Z.L.; Yu, Q.; Cui, J.P.; Qi, K.; Chen, Z.J.; Cao, Z.P.; Yang, P. Thermal history and its controls on oil and gas of the Ordos Basin. *Earth Sci. Front.* **2017**, *24*, 137–148. [CrossRef]
49. Wan, Z.L.; Wei, L.; Wan, X.Z.; Wan, N.X.; Fan, C.Y.; Li, Y.J.; Zhao, X.J.; Zhao, X.D.; Ren, L.Y.; Cao, H.X. Accumulation process and mechanism of Lower Paleozoic gas reservoir in Yan'an area, Ordos Basin. *Acta Pet. Sin.* **2016**, *36*, 99–110. [CrossRef]
50. Tao, H.; Cui, J.P.; Zhao, F.F.; Ren, Z.L.; Qi, K.; Liu, H.; Su, S.H. Thermal History and Hydrocarbon Accumulation Stages in Majiagou Formation of Ordovician in the East-Central Ordos Basin. *Energies* **2024**, *17*, 4435. [CrossRef]

Disclaimer/Publisher's Note: The statements, opinions and data contained in all publications are solely those of the individual author(s) and contributor(s) and not of MDPI and/or the editor(s). MDPI and/or the editor(s) disclaim responsibility for any injury to people or property resulting from any ideas, methods, instructions or products referred to in the content.